A non-self-consistent range-separated time-dependent density functional approach for large-scale simulations

2012 J. Phys.: Condens. Matter 24 205801

(http://iopscience.iop.org/0953-8984/24/20/205801)

J. Phys.: Condens. Matter **24** (2012) 205801 (8pp) doi:10.1088/0953-8984/24/20/205801

A non-self-consistent range-separated time-dependent density functional approach for large-scale simulations

Xu Zhang, Zi Li and Gang Lu

Department of Physics and Astronomy, California State University Northridge, Northridge, CA 91330-8268, USA

E-mail: ganglu@csun.edu

Received 20 January 2012, in final form 14 March 2012
Published 18 April 2012
Online at stacks.iop.org/JPhysCM/24/205801

Abstract

We propose an efficient method for carrying out time-dependent density functional theory (TDDFT) calculations using range-separated hybrid exchange–correlation functionals. Based on a non-self-consistent range-separated Hamiltonian, the method affords large-scale simulations at a fraction of the computational time of conventional hybrid TDDFT approaches. For typical benchmark molecules including N_2, CO, C_6H_6, H_2CO and the C_2H_4–C_2F_4 dimer, the method possesses the same level of accuracy as the conventional approaches for the valence, Rydberg, and charge-transfer excitation energies when compared to the experimental results. The method is used to determine $\pi \rightarrow \pi^*$ excitations in both disordered and crystalline poly(3-hexylthiophene) (P3HT) conjugated polymers with more than six hundred atoms and it yields excitation energies and charge densities that are in excellent agreement with experiments. The simulation of the crystalline P3HT reveals that the phase of the wavefunctions could have an important effect on the excitation energy; a hypothesis based on π–π stacking is proposed to explain this novel effect in conjugated polymers.

(Some figures may appear in colour only in the online journal)

1. Introduction

The last decade has witnessed the emergence of time-dependent density functional theory (TDDFT) [1, 2] as one of the most popular theoretical/computational tools for understanding electronic excitations. An important advantage of TDDFT over many-body Green's function or traditional wavefunction based theories is the density dependence of TDDFT energy functionals, which is formally exact. However, in practice, approximate exchange–correlation (XC) functionals have to be used, such as the adiabatic local density approximation (LDA) or the generalized gradient approximations (GGA). For example, the gradient-corrected BP86 [3, 4] and hybrid B3LYP [5, 6] functionals have been used extensively, providing reliable ground state properties. However, among other problems, these functionals fail to exhibit the long-range $-1/r$ dependence of the exchange–correlation potential on the inter-electronic distance r; as a result they have serious problems, such as in dealing with extended Rydberg states [7, 8] and charge-transfer excitations [9, 10]. Although asymptotically corrected XC functionals such as LB94 lead to a better description of Rydberg states, they still significantly underestimate the charge-transfer states [11]. To remedy this crucial deficiency, range-separated (RS) hybrid XC functionals [12–16] have been proposed for smoothly recovering the correct asymptotic behavior of the XC potential at large distances and simultaneously maintaining the delicate balance between the exchange and correlation contributions at short distances. The range-separated functionals have been shown to yield substantial improvement over the local or conventional hybrid functionals for excitations in conjugated polymers [17–22], weakly bonded complexes [23, 24] and extended charge-transfer states [25–29], to name but a few.

Despite the success of the range-separated TDDFT (RS-TDDFT), its application to large systems remains challenging due to the overwhelming computational cost of the Hartree–Fock (HF) integrals, which are 30–50 times more expensive than the conventional functionals. For dynamical simulations, the RS-TDDFT is normally

limited to a few tens of atoms with moderate computational resources. To overcome the prohibitive computational barrier, herein we propose an efficient RS-TDDFT method based on a non-self-consistent range-separated Hamiltonian that can deal with excitations in large systems (up to 10^3 atoms) with a reasonable computational cost and a desirable accuracy. In this approach, the non-self-consistent range-separated Hamiltonian is used to determine the excited wavefunctions and energies following Casida's formulation [30]. Two key approximations are introduced. (1) The KS orbitals and energies are determined non-self-consistently by diagonalizing the range-separated KS Hamiltonian constructed from a self-consistent KS-GGA calculation. The range-separated Hamiltonian is not updated self-consistently; thus the time-consuming HF exchange integrals are calculated only once to determine the KS orbitals and energies. (2) Since we are primarily interested in low-energy excitations contributed from the frontier KS orbitals, we consider only a subspace of occupied KS orbitals in determining the energies and wavefunctions of the frontier KS orbitals. For a similar level of accuracy, the first approximation could produce saving of one order of magnitude in computational time comparing to the conventional range-separated TDDFT methods; the second approximation can further reduce the computational time and memory up to one order of magnitude.

Recently, the optoelectronic and photovoltaic technologies have broadened their materials base to organic molecules, and in particular to π-conjugated oligomers and polymers, thanks to their unique nonlinear optical and/or semiconducting properties, paving the way to the emergence of organic optoelectronics [31]. One of the prominent examples is poly(3-hexylthiophene) (P3HT) which is the focus of the present study. P3HT has been widely used in organic electronics, including as the donor material in bulk heterojunction organic solar cells. Light absorption within P3HT generates excitons that diffuse to the donor/acceptor interfaces where they dissociate into free charge carriers. Therefore an accurate description of the excitons in P3HT is of crucial importance in understanding exciton generation, diffusion and dissociation in P3HT and related materials. To study excitations in either amorphous or crystalline P3HT—both are important for applications—large-scale TDDFT simulations are indispensable. Therefore it is of great scientific interest to develop efficient computational methods that can describe excitations accurately in large organic molecules and crystals. Our results show that the local or semi-local functionals fail to provide an accurate description of the exciton states in P3HT, which can be addressed satisfactorily by using the range-separated hybrid functionals.

2. Methodology

In range-separated XC functionals, the Coulomb repulsion operator $1/r_{12}$ is divided into short-range and long-range parts by using the error function:

$$\frac{1}{r_{12}} = \frac{\mathrm{erfc}(\mu r_{12})}{r_{12}} + \frac{\mathrm{erf}(\mu r_{12})}{r_{12}}, \tag{1}$$

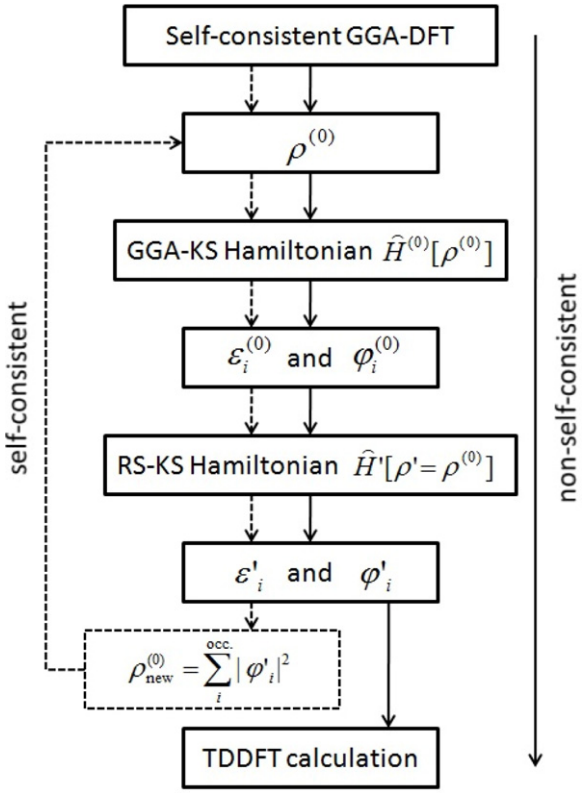

Figure 1. The schematic flowchart of the proposed approach (non-self-consistent; solid line) and the self-consistent RS-DFT calculation (dashed line).

where $r_{12} = |\mathbf{r}_1 - \mathbf{r}_2|$ is the distance between two electrons at $\mathbf{r}_1$ and $\mathbf{r}_2$, and μ is a range-separation parameter. The range-separated XC functionals are given by [13, 14]

$$E'_{\mathrm{xc}} = E_{\mathrm{c,DFT}} + E^{\mathrm{SR}}_{\mathrm{x,DFT}} + E^{\mathrm{LR}}_{\mathrm{x,HF}}, \tag{2}$$

where $E_{\mathrm{c,DFT}}$ is the DFT correlation; $E^{\mathrm{SR}}_{\mathrm{x,DFT}}$ is the short-range part of the conventional DFT exchange functional, and $E^{\mathrm{LR}}_{\mathrm{x,HF}}$ is the long-range part of the HF exchange integral. Since $E_{\mathrm{x,DFT}} \equiv E^{\mathrm{SR}}_{\mathrm{x,DFT}} + E^{\mathrm{LR}}_{\mathrm{x,DFT}}$, where $E^{\mathrm{LR}}_{\mathrm{x,DFT}}$ is the long-range part of the conventional DFT exchange functional, equation (2) can be rewritten as $E'_{\mathrm{xc}} = E_{\mathrm{xc,DFT}} - E^{\mathrm{LR}}_{\mathrm{x,DFT}} + E^{\mathrm{LR}}_{\mathrm{x,HF}}$. Then the corresponding XC effective potential is given by $\hat{V}'_{\mathrm{xc}} = \hat{V}_{\mathrm{xc,DFT}} - \hat{V}^{\mathrm{LR}}_{\mathrm{x,DFT}} + \hat{V}^{\mathrm{LR}}_{\mathrm{x,HF}}$.

To introduce the approximations, let us start with the self-consistent range-separated DFT calculations with the KS eigenvalues and eigenfunctions obtained by conventional GGA-DFT. The schematic flowchart of the self-consistency is shown in figure 1 by a dashed line. Here $\rho^{(0)}$, $\hat{H}^{(0)}[\rho^{(0)}]$, $\epsilon_i^{(0)}$, and $\varphi_i^{(0)}$ denote the charge density, KS Hamiltonian, KS eigenvalue, and KS eigenfunction from the self-consistent GGA-DFT calculations and ρ', $\hat{H}'[\rho']$, ϵ'_i, and φ'_i represent the same quantity in the RS-DFT formulation. A self-consistent GGA calculation is performed to determine the ground state density $\rho^{(0)}$ and the corresponding GGA-KS Hamiltonian. The eigenvalues and eigenfunctions of the Hamiltonian can then be obtained, which are used to construct the range-separated KS (RS-KS) Hamiltonian in equation (3).

More specifically, the RS-KS Hamiltonian matrix elements are expressed in terms of the GGA quantities as

$$\begin{aligned}\hat{H}'_{ij} &= \langle\varphi_j^{(0)}|\hat{H}'|\varphi_i^{(0)}\rangle = \langle\varphi_j^{(0)}|\hat{H}^{(0)} - \hat{V}^{\mathrm{LR}}_{\mathrm{x,DFT}} + \hat{V}^{\mathrm{LR}}_{\mathrm{x,HF}}|\varphi_i^{(0)}\rangle \\ &= \epsilon_i^{(0)}\delta_{ij} - \int \varphi_j^{(0)*}(\mathbf{r}) V^{\mathrm{LR}}_{\mathrm{x,DFT}}[\rho^{(0)}(\mathbf{r})]\varphi_i^{(0)}(\mathbf{r})\,\mathrm{d}\mathbf{r} \\ &\quad - \sum_k^{\mathrm{occ}} \left[n_{jk} \left| \frac{\mathrm{erf}(\mu r)}{r} \right| n^*_{ik} \right], \end{aligned} \tag{3}$$

where the charge density is defined as $n_{ik} \equiv \varphi_i^{(0)*}\varphi_k^{(0)}$ and the Coulomb inner product is defined as $[f|\frac{1}{r}|g] \equiv \int \frac{f(\mathbf{r}_1)g(\mathbf{r}_2)}{|\mathbf{r}_1-\mathbf{r}2|}\,\mathrm{d}\mathbf{r}_1\,\mathrm{d}\mathbf{r}_2$. Here, i and j denote both the occupied and virtual orbitals, and k indicates only the occupied orbitals. The range-separated KS eigenvalue ϵ'_i and eigenfunction φ'_i can thus be determined by a direct diagonalization of the Hamiltonian matrix $\hat{H}'$ in equation (3). A new charge density can be computed by using $\rho^{(0)}_{\mathrm{new}} = \sum_i^{\mathrm{occ}} \varphi'^*_i\varphi'_i$. The updated $\rho^{(0)}_{\mathrm{new}}$, $\epsilon^{(0)}_{i,\mathrm{new}}$ and $\varphi^{(0)}_{i,\mathrm{new}}$ are then used to construct the new range-separated Hamiltonian and the cycle repeats until the converged ρ', ϵ'_i and φ'_i are obtained.

As the first approximation in the method, we assume the ground state charge density $\rho^{(0)}$ obtained by the KS-GGA to be the same as ρ' determined from RS-DFT; this is a reasonable approximation because the GGA functionals are known to produce accurate ground state charge densities. Therefore instead of executing the self-consistent loop, we perform a non-self-consistent RS-DFT calculation to obtain ϵ'_i and φ'_i without updating the RS-DFT Hamiltonian in equation (3). The flowchart of the non-self-consistent method is shown in figure 1 with solid lines. We should point out that there are well-known situations where the ground state charge density of KS-GGA deviates significantly from that of RS-DFT. For example, when a molecule is being stretched or subject to an applied electric field or when charge transfer takes place between the molecule and metal leads [32], one should be particularly cautious in using the non-self-consistent RS-DFT method.

Using the non-self-consistently determined RS-DFT eigenvalues and eigenfunctions, the excited energies and states can be subsequently determined by solving the non-Hermitian eigenvalue equations of Casida [30]:

$$\begin{pmatrix} \mathbf{A} & \mathbf{B} \\ \mathbf{B}^* & \mathbf{A}^* \end{pmatrix} \begin{pmatrix} \mathbf{X} \\ \mathbf{Y} \end{pmatrix} = \omega \begin{pmatrix} \mathbf{1} & \mathbf{0} \\ \mathbf{0} & -\mathbf{1} \end{pmatrix} \begin{pmatrix} \mathbf{X} \\ \mathbf{Y} \end{pmatrix}, \tag{4}$$

where ω is the excitation energy and the elements of matrices $\mathbf{A}$ and $\mathbf{B}$ are given by

$$\begin{aligned} A_{ij\sigma,kl\tau} &= \delta_{i,k}\delta_{j,l}\delta_{\sigma,\tau}(\epsilon'_{j\sigma} - \epsilon'_{i\sigma}) + K_{ij\sigma,kl\tau}, \\ B_{ij\sigma,kl\tau} &= K_{ij\sigma,lk\tau}. \end{aligned} \tag{5}$$

Here, i, k and j, l indicate the occupied and virtual orbitals, respectively. σ and τ are spin indices. And the coupling matrix elements $K_{ij\sigma,kl\tau}$ are given by

$$\begin{aligned} K_{ij\sigma,kl\tau} &= \left[n'_{ij\sigma} \left| \frac{1}{r} \right| n'^*_{kl\tau} \right] - \delta_{\sigma\tau} \left[n'_{ik\sigma} \left| \frac{\mathrm{erf}(\mu r)}{r} \right| n'^*_{jl\tau} \right] \\ &\quad + \int n'_{ij\sigma}(\mathbf{r}_1) \frac{\delta^2(E_{\mathrm{xc,DFT}} - E^{\mathrm{LR}}_{\mathrm{x,DFT}})}{\delta\rho^{(0)}_\sigma(\mathbf{r}_1)\delta\rho^{(0)}_\tau(\mathbf{r}_2)} n'^*_{kl\tau}(\mathbf{r}_2)\,\mathrm{d}\mathbf{r}_1\,\mathrm{d}\mathbf{r}_2, \end{aligned} \tag{6}$$

where $n'_{ij\sigma} \equiv \varphi'^*_{i\sigma}\varphi'_{j\sigma}$. The last two terms on the right-hand side of equation (6) represent the linear response of the nonlocal HF exchange energy and the local XC potential with respect to variations of the density matrix, respectively [30].

Because the GGA quantities are used in constructing the non-self-consistent RS-DFT Hamiltonian, and subsequently the calculations of excited states, the proposed method can be considered as an improvement over GGA-TDDFT, making a passage towards RS-TDDFT.

According to the assignment ansatz of Casida, the many-body wavefunction of an excited state I can be written as [30]

$$\Phi_I \approx \sum_{ij\sigma} z_{I,ij}\hat{a}^\dagger_{j\sigma}\hat{a}_{i\sigma}\,\Phi_0, \tag{7}$$

where $z_{I,ij} = (\mathbf{X}_{I,ij} + \mathbf{Y}_{I,ij})/\sqrt{\omega_I}$; $\hat{a}_{i\sigma}$ is the annihilation operator acting on the ith KS orbital with spin σ and Φ_0 is the ground state many-body wavefunction taken to be the single Slater determinant of the occupied KS orbitals. With the density operator $\hat{\rho}(\mathbf{r}) = \sum_{n=1}^N \delta(\mathbf{r} - \mathbf{r}_n)$ of an N-electron system, the charge density of the Ith excited states can be written as [33]

$$\begin{aligned} \rho^I_{\mathrm{excited}}(\mathbf{r}) &= \langle\Phi_I|\hat{\rho}(\mathbf{r})|\Phi_I\rangle = \rho_{\mathrm{ground}}(\mathbf{r}) \\ &\quad + \sum_{i,jj'} z^*_{I,ij}z_{I,ij'}\phi^*_j(\mathbf{r})\phi_{j'}(\mathbf{r}) - \sum_{ii',j} z^*_{I,ij}z_{I,i'j}\phi^*_{i'}(\mathbf{r})\phi_i(\mathbf{r}). \end{aligned} \tag{8}$$

Here, ρ_{ground} is the charge density of the ground state, and the second and the third terms on the right-hand side of equation (8) represent the charge density of the quasi-electron and the quasi-hole, respectively.

3. Validations

In the following, we validate the proposed method by comparing the excitation energies of five molecules (N_2, CO, C_6H_6, H_2CO and C_2H_4–C_2F_4) to the conventional RS-TDDFT results and the corresponding experimental values. These molecules are typically used in benchmarking the accuracy of TDDFT calculations [13]. The KS-GGA calculations with the projector augmented wave pseudopotentials [34] and Perdew–Burke–Ernzerhof (PBE) [35] XC functional are performed at the Γ point with an energy cutoff 300 eV [36, 37]. The molecules are placed in an orthorhombic box with the dimensions of $20 \times 20 \times 20$ Å^3 using the periodic boundary conditions. The dimension of the simulation box is increased to 30 Å for the C_2H_4–C_2F_4 dimer. Experimental geometries of these molecules have been used in the TDDFT calculations. The range-separation parameter μ varies for different systems and it can be tuned by enforcing the identity between the energy of the highest occupied molecular orbital (HOMO) and the ionization potential [38].

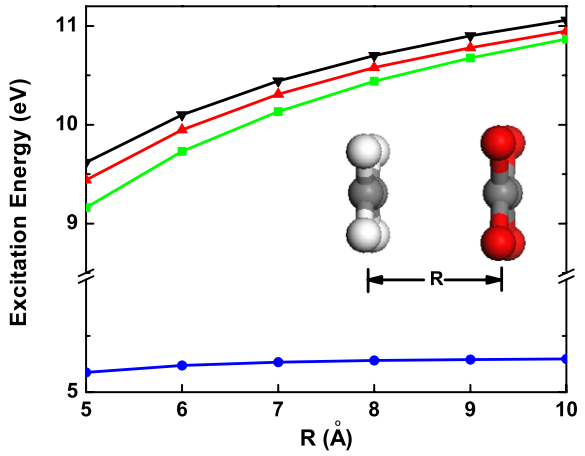

Figure 2. The lowest charge-transfer excitation energy of the C_2H_4–C_2F_4 dimer versus intermolecular distance R. The red, green, and blue curves represent the results determined from the conventional range-separated TDDFT, the proposed method, and the PBE-GGA functional, respectively. The experimental values (black curve) are estimated by the function $c_0 - 1/R$, where $c_0 = 12.5$ eV is the energy difference between the vertical ionization potential of C_2H_4 and the electron affinity of C_2F_4. Inset: the atomic structure of the C_2H_4–C_2F_4 dimer where gray, white, and red spheres denote C, H, and F atoms, respectively.

Here μ is taken to be 0.62 Å^{-1}, which has been previously optimized for the benchmark molecules [13].

The vertical excitation energies of N_2, CO, C_6H_6 and H_2CO determined by the proposed method and the conventional RS-TDDFT method, and the corresponding experimental values, are listed in table 1. To assess the overall accuracy of the proposed method, we have determined the mean absolute errors (MAE) for the valence and Rydberg excitations. Comparing to the experiment values, the MAEs for the valence and the Rydberg excitations from the proposed method are 0.24 eV and 0.28 eV, respectively, less than the corresponding MAE values of the conventional RS-TDDFT of 0.27 and 0.65 eV. Therefore, the proposed method has a similar accuracy to the conventional RS-TDDFT for the valence states and is more accurate than the conventional RS-TDDFT for the Rydberg excitations. The superior performance of the proposed method for the Rydberg states may be due to fortuitous error cancellations: on one hand, the conventional RS-TDDFT is known to underestimate the Rydberg energies; on the other hand, the non-self-consistent RS-DFT calculation typically yields higher energies than the fully self-consistent calculation (a variational principle at work). We have also calculated the lowest charge-transfer excitation energy of the C_2H_4–C_2F_4 dimer with increasing intermolecular distance as shown in figure 2. The results demonstrate that the PBE-GGA functional (blue dotted curve) fails to describe the long-range behavior of the charge-transfer excitation energies, but the proposed method gives results (green squared curve) that agree very well with the conventional RS-TDDFT results (red curve) and reproduces the correct long-range behavior of the experiment (black curve).

Table 1. Vertical excitation energies (in eV) of N_2, CO, C_6H_6 and H_2CO molecules calculated by the proposed method ('Ours') in comparison with the conventional RS-TDDFT calculations ('Conventional') and the experiments ('Exp.') in [13]. Here, 'V' and 'R' represent the valence and Rydberg excitations, respectively.

	State	Ours	Conventional	Exp.
N_2	V: $^1\Pi_g$ ($\sigma_g \to \pi_g$)	9.44	9.34	9.31
	V: $^1\Sigma_u^-$ ($\pi_u \to \pi_g$)	9.44	9.34	9.92
	V: $^1\Delta_u$ ($\pi_u \to \pi_g$)	10.04	9.89	10.27
	R: $^1\Sigma_g^+$ ($\sigma_g \to 3s\sigma_g$)	11.69	11.57	12.20
	R: $^1\Pi_u$ ($\sigma_g \to 3p\pi_u$)	12.91	12.05	12.90
	R: $^1\Sigma_u^+$ ($\sigma_g \to 3p\pi_u$)	12.94	12.09	12.98
	V: $^3\Sigma_u^+$ ($\pi_u \to \pi_g$)	7.51	7.41	7.75
	V: $^3\Pi_g$ ($\sigma_g \to \pi_g$)	7.85	7.78	8.04
	V: $^3\Delta_u$ ($\pi_u \to \pi_g$)	8.61	8.32	8.88
	V: $^3\Sigma_u^-$ ($\pi_u \to \pi_g$)	9.44	9.34	9.67
	V: $^3\Pi_u$ ($\sigma_u \to \pi_g$)	10.95	10.77	11.19
	R: $^3\Sigma_g^+$ ($\sigma_g \to 3s\sigma_g$)	11.24	11.14	12.00
CO	V: $^1\Pi$ ($\sigma \to \pi^*$)	8.69	8.43	8.51
	V: $^1\Sigma^-$ ($\pi \to \pi^*$)	9.84	9.77	9.88
	V: $^1\Delta$ ($\pi \to \pi^*$)	10.30	10.21	10.23
	R: $^1\Sigma^+$ ($\sigma \to 3s$)	10.50	10.28	10.78
	R: $^1\Sigma^+$ ($\sigma \to 3p\sigma$)	11.68	10.73	11.40
	R: $^1\Pi$ ($\sigma \to 3p\pi$)	11.87	10.83	11.53
	V: $^3\Pi$ ($\sigma \to \pi^*$)	6.05	6.06	6.32
	V: $^3\Sigma^+$ ($\pi \to \pi^*$)	8.32	8.23	8.51
	V: $^3\Delta$ ($\pi \to \pi^*$)	9.20	8.95	9.36
	V: $^3\Sigma^-$ ($\pi \to \pi^*$)	9.84	9.77	9.88
	R: $^3\Sigma^+$ ($\sigma \to 3s$)	10.05	8.95	10.40
	R: $^3\Sigma^+$ ($\sigma \to 3p\sigma$)	11.31	9.79	11.30
C_6H_6	V: $1\,^1B_{2u}$ ($\pi \to \pi^*$)	5.49	5.39	4.90
	V: $1\,^1B_{1u}$ ($\pi \to \pi^*$)	6.73	6.22	6.20
	V: $1\,^1E_{1u}$ ($\pi \to \pi^*$)	7.08	7.00	6.94
	R: $1\,^1E_{1g}$ ($\pi \to 3s$)	7.21	6.70	6.33
	R: $1\,^1A_{2u}$ ($\pi \to 3p\sigma$)	7.37	7.16	6.93
	R: $1\,^1E_{2u}$ ($\pi \to 3p\sigma$)	7.38	7.31	6.95
	V: $1\,^3B_{1u}$ ($\pi \to \pi^*$)	4.18	3.76	3.94
	V: $1\,^3E_{1u}$ ($\pi \to \pi^*$)	4.79	4.81	4.76
	V: $1\,^3B_{2u}$ ($\pi \to \pi^*$)	5.06	5.03	5.60
H_2CO	V: $^1A_2$ ($n \to \pi^*$)	3.98	3.81	3.94
	V: $^1B_1$ ($\sigma \to \pi^*$)	9.21	9.10	8.68
	R: $^1B_2$ ($n \to 3sa_1$)	6.92	6.71	7.09
	R: $^1A_1$ ($n \to 3pb_2$)	7.96	7.54	7.97
	R: $^1B_2$ ($n \to 3pa_1$)	7.90	7.45	8.12
	R: $^1A_2$ ($n \to 3pb_1$)	8.61	7.69	8.38
	V: $^3A_2$ ($n \to \pi^*$)	3.39	3.13	3.50
	V: $^3A_1$ ($\pi \to \pi^*$)	5.99	5.84	5.53
	R: $^3B_2$ ($n \to 3sa_1$)	6.63	6.57	6.83
	R: $^3A_1$ ($n \to 3pb_2$)	7.85	7.44	7.79
	R: $^3B_2$ ($n \to 3pa_1$)	7.73	7.30	7.96

4. Applications to the conjugated polymer P3HT

In typical spectroscopic measurements and realistic applications involving large molecules, only low-energy excitations are of particular interest; these low-energy excitations correspond to electron transitions from shallow occupied orbitals to low-energy virtual orbitals. Herein we consider the low-energy excitations from N_o occupied orbitals to N_v virtual

orbitals, i.e., the occupied KS orbitals from HOMO$-N_{\rm o}+1$ to HOMO and the virtual KS orbitals from LUMO to LUMO $+$ $N_{\rm v}-1$ are included in the calculations of equation (4). In π-conjugated polymers, the frontier orbitals (including both occupied and virtual levels near the Fermi energy) are composed of π orbitals while the deep occupied states consist of σ orbitals. Since there is negligible spatial overlap between the π and σ orbitals, the contribution from the σ orbitals to both the HF and DFT exchange energies can be neglected. Hence, we make the second approximation by ignoring the contributions from the deep σ orbitals in the last two terms of equation (3), i.e., the summation of k includes $N_{\rm o}+N_{\rm os}$ where $N_{\rm os}$ is the number of additional occupied orbitals below the $N_{\rm o}$ occupied orbitals. Moreover, in the second term, $\rho^{(0)}(\mathbf{r})$ is replaced by $\sum_i^{N_{\rm o}+N_{\rm os}} n_{ii}(\mathbf{r})$. The KS eigenvalues ϵ_i' are then obtained by diagonalizing the Hamiltonian matrix $\hat{H}'_{ij}$ whose dimension is $N_{\rm o}+N_{\rm v}$.

To assess the errors of the second approximation in large molecules, we calculate the excitation energies of disordered P3HT polymers. A cubic computational cell with a dimension of 18.2 Å is used in the range-separated TDDFT calculations. The supercell contains 606 atoms, including three P3HT chains; each chain consists of eight thiophene rings leading to a mass density of 1.1 g cm^{-3}, similar to the experimental value [39]. The initial atomic structure of the P3HT chains is obtained from randomly placed and warped configurations, and is then subject to a full atomic relaxation to reach a local energy minimum. We find that $\mu = 0.62$ Å^{-1} also works well for P3HT, which has been used in the following calculations. $N_{\rm o} = 6$ occupied orbitals and $N_{\rm v} = 9$ virtual orbitals are included in the calculation of equation (4). A series of TDDFT calculations are performed by increasing $N_{\rm os}$ from 1 to 717 (for $N_{\rm os} = 717$, all occupied orbitals are included). The KS eigenvalues ($\epsilon_i'^{\rm ref}$) and excitation energies ($\omega^{\rm ref}$) determined with $N_{\rm os} = 717$ are taken as reference points for evaluating the errors. The error in the KS eigenvalues is given by $\Delta\epsilon_{\rm o\ (v)}$ defined as $\Delta\epsilon_{\rm o\ (v)} = \sqrt{\sum_i^{N_{\rm o\ (v)}} (\epsilon_i' - \epsilon_i'^{\rm ref})^2 / N_{\rm o\ (v)}}$ for the occupied (o) and virtual orbitals (v), respectively. The error in the excitation energy is represented by $\Delta\omega_{\rm S(T)} = \omega_{\rm S(T)} - \omega^{\rm ref}_{\rm S(T)}$ for the lowest singlet (S) and triplet (T) excitation, respectively. The errors as a function of $N_{\rm os}$ are displayed in figure 3. It is found that the errors decrease precipitously across $N_{\rm os} = 49$ and then approach the reference points gradually. At $N_{\rm os} = 49$, ϵ_i' amounts to 80% of $\epsilon_i'^{\rm ref}$ and $\omega_{\rm S(T)}$ is about 85% of $\omega^{\rm ref}_{\rm S(T)}$. Thus $N_{\rm os} = 49$ represents an excellent trade-off point—one can attain the accuracy of 85% for the excitation energies with ∼15 times less computational cost comparing to the reference points. Because there are 48 π orbitals in P3HT from 96 C atoms along the backbone, taking $N_{\rm os} = 49$ ensures that all π orbitals are included. These ignored orbitals are σ only, which have negligible overlap with the π orbitals; thus their contribution to equation (3) can be neglected.

The failures in TDDFT with the conventional or hybrid XC functionals often show up in the lowest-lying $\pi \rightarrow \pi^*$ excited state [40, 41], including the charge density distribution. With $N_{\rm os} = 49$, we have determined the charge density difference between the lowest excited state and the ground state for the disordered P3HT polymer (the lowest excited state of P3HT is that of the $\pi \rightarrow \pi^*$ transition) using both the PBE-GGA functional and the range-separated functional. In figure 4, the positive value represents an accumulation of the charge density (or the formation of the quasi-electron) and the negative value indicates a depletion of the charge density (or the formation of the quasi-hole). It is evident that the range-separated functional yields an intra-chain excitation and the quasi-electron and the quasi-hole are located in the same P3HT chain; on the other hand, the PBE-GGA functional predicts an inter-chain excitation and the quasi-electron and the quasi-hole are separated in different P3HT chains. The intra-chain excitation result is consistent with experiments where the Frenkel-like intra-chain excitons have been observed in the disordered P3HT as the lowest excitation [42–44]. Therefore the proposed method is capable of providing an accurate description of the excited states in P3HT in terms of charge density.

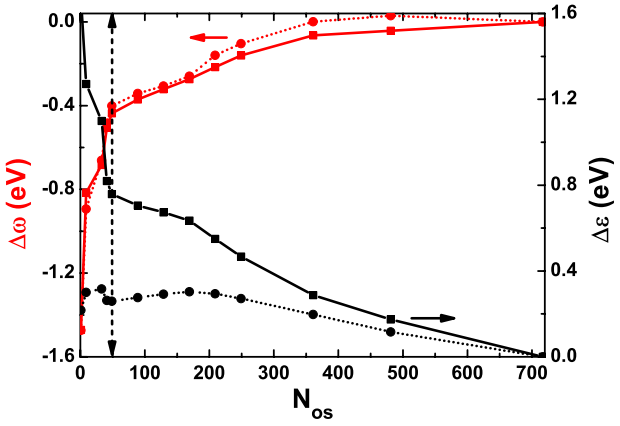

Figure 3. Errors in the excitation energy (left) and KS eigenvalues (right) versus $N_{\rm os}$ for the disordered P3HT. The red solid (dot) curve represents the errors of the lowest singlet (triplet) excitation energy. The black solid (dot) curve denotes the errors of the occupied (virtual) KS eigenvalues.

Since the proposed method uses a plane-wave basis with periodic boundary conditions, it can be applied to model periodic systems such as organic crystalline semiconductors. Some of these semiconductors exhibit great potential in photovoltaic applications thanks to their macroscopic exciton diffusion lengths [45]. In the following, we use the proposed method to study the lowest singlet excitation in crystalline P3HT. This excitation involves the transition between the delocalized π and π^* states, which takes place over the entire P3HT chains [46]. It has been observed that this excitation energy depends crucially on the conjugation length of the polymers—the longer the conjugation length, the more closely the energy approaches the experimental value [46]. In addition, there is also π–π stacking interaction between the polymer chains, which has to be included in the simulations. To examine the effect of the conjugation length and the π–π stacking on the excitation energy, we have considered eight different models divided into two groups. In group I, a single P3HT chain is contained in the supercell while there

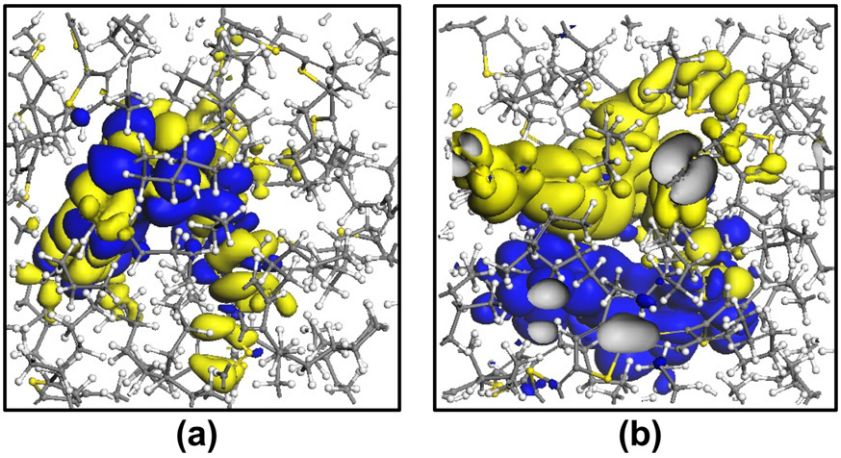

Figure 4. Charge density difference ($\rho_{\text{excited}} - \rho_{\text{ground}}$) between the lowest excited state and the ground state determined by (a) the proposed method and (b) the PBE-GGA functional in the disordered P3HT. The blue (yellow) iso-surfaces illustrate the charge density difference at $+0.0005$ (-0.0005) Å^{-3}. The positive (negative) charge density corresponds to the quasi-electron (hole). The gray, white, and yellow spheres denote C, H, and S atoms, respectively.

are two P3HT chains in the supercell for group II. In each group, different boundary conditions along the z (stacking) and x (chain) directions are used. To simulate a finite P3HT segment, a vacuum is placed along the x direction (H atoms are introduced to saturate the dangling bonds along the x direction); to simulate an infinite chain, no vacuum is used. Similarly, to simulate an isolated single or double P3HT chain, a vacuum is introduced along the z direction; to simulate the stacking interaction between the chains, no vacuum is placed along the z direction.

With $N_{\text{o}} = 8$ and $N_{\text{v}} = 8$, we have calculated the lowest excitation energy for the eight models and the results are summarized in table 2. Firstly, we find that the excitation energy of the finite P3HT segment is much higher than that of the infinite chain(s). There are two reasons for the energy difference: (1) the presence of saturating H atoms in the finite segment increases the KS gap which amounts to 25% of the increased excitation energy; (2) the Coulomb interaction between the quasi-electron and the quasi-hole is lower in the finite P3HT segment, and leads to 75% increase of the excitation energy. The second reason can be explained by comparing figures 5(b) and (c): there is an attractive interaction between the quasi-electron and quasi-hole across the boundaries in figure 5(b), while such interaction is absent in figure 5(c). Since the stronger the Coulomb attraction, the lower the excitation energy, the infinite chain(s) has a lower energy than the segment. Secondly, we find that comparing to the isolated single chain, the stacked chains raise the excitation energy by 0.54 eV. In contrast, comparing to the isolated double chain, the stacked chains lower the excitation energy by 0.35 eV. Accordingly, we estimate the lowest excitation energy of the crystalline P3HT to range from 1.5 eV (from the double-chain calculation) to 2.4 eV (from the single-chain calculation), which is in line with the experimental value at ∼2.0 eV [46]. The two cases (single chain versus double chain) have the same atomic structure and charge density; in fact, since the calculation

Table 2. The lowest singlet excitation energies (in eV) determined for the eight P3HT models.

	Group I		Group II	
z:	Isolated	Stacking	Isolated	Stacking
x: segment	3.45	3.99	3.03	2.51
x: infinite	1.91	2.45	1.81	1.46

is performed at the Γ point, their wavefunctions also have the same amplitude. However, their wavefunctions acquire different phases because the periodic boundary condition or the Born–von Karman condition is applied differently (upon different boxes). Therefore the phase of the wavefunctions could have a significant effect (∼0.8 eV in this case) on the excitation energy, notwithstanding it not affecting the ground state energy. To shed light on the phase effect, in figure 5 we present a schematic picture of π–π stacking between the polymer chains including three periodic cells for both single chain and double chain. The π–π interaction is highlighted by the red dashed lines. Note that the wavefunctions have a difference in phases between the single and double chain. In fact, the configuration shown in (b) is the only possible one that would yield a different phase from (a). For the single chain the π–π stacking involves the opposite-signed p orbitals, while for the double chain, the π–π stacking consists of the same-signed p orbitals. Hence we speculate that the same-signed π–π stacking leads to a lower excitation energy. Further theoretical or experimental investigations are required to validate the speculation unambiguously. A recent work by Nakatsuka *et al* [47] has found that the slipping modes could also change the excitation energies significantly in π-stacking molecules. We note that the slipping modes could weaken the π–π stacking between the polymer chains which may either increase or decrease the excitation energies, depending on the π–π stacking phase.

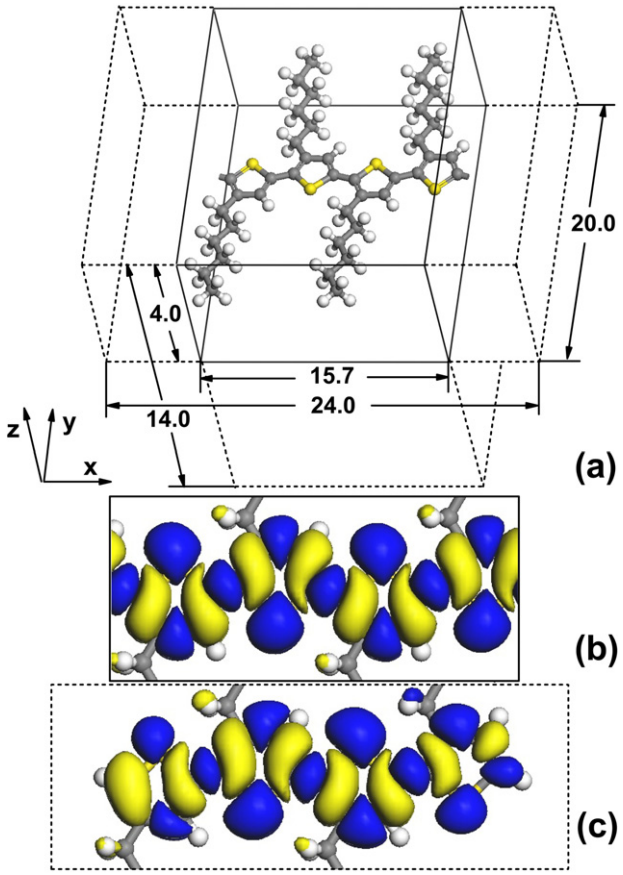

Figure 5. (a) The P3HT molecule is placed in the solid box and the vacuum layers are contained in the dashed box along both x and z directions. Periodic boundary conditions are applied in all three directions. The polymer chain is along the x direction and the inter-chain stacking is along the z direction. The dimensions of the periodic boxes are given in Å. The gray, white, and yellow spheres denote C, H, and S atoms, respectively. The electron density difference between the lowest excited state and the ground state is shown for the infinite P3HT chains (b) and the finite P3HT segment (c). The blue (yellow) iso-surfaces illustrate the charge density difference at $+0.001$ (-0.001) Å^{-3}.

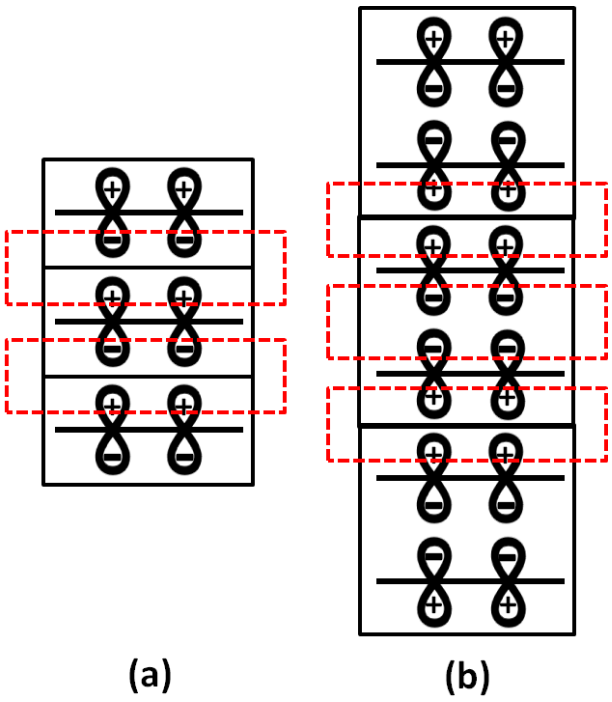

Figure 6. Schematic picture of π–π stacking in the single-chain (a) and double-chain (b) supercells. Three periodic supercells (solid boxes) are shown for each case, and the red dashed lines denote the π–π stacking. The solid lines represent the P3HT chains.

5. Conclusions

In this paper, we have proposed an efficient method based on the non-self-consistent RS-DFT Hamiltonian for large-scale TDDFT calculations. The excitation energies (including valence, Rydberg, and charge-transfer excited states) of typical benchmark molecules show excellent agreement with experiments. The method is used to simulate the disordered P3HT polymer with more than six hundred atoms and the computational errors are evaluated. The method shows that the lowest excitation of the disordered P3HT is an intra-chain exciton, consistent with the experimental observations. We have also calculated the excitation energy for the crystalline P3HT and found that increasing the conjugation length of the polymer lowers the excitation energy. More interestingly, the π–π stacking between the polymer chains exhibits an intriguing phase effect on the excitation energy. The proposed method yields a lowest excitation energy for the crystalline P3HT that agrees well with the experimental value. Overall, for the systems examined here, the proposed method can reach a similar accuracy to the conventional RS-TDDFT method but at a small fraction of the computational cost. However, the general validity of the method has yet to be established beyond the conjugated polymers and the benchmark molecules. Although the method is not proposed as a replacement for the conventional RS-TDDFT approaches, it can be used as an alternative—sometimes the only one—for treating large systems that are beyond the reach of the conventional methods. We hope that the encouraging results reported here will inspire further research in this direction.

Acknowledgment

This work was supported by the Office of Naval Research (N00014-11-1-0175).

References

[1] Runge E and Gross E K U 1984 *Phys. Rev. Lett.* **52** 997
[2] Gross E K U and Kohn W 1990 *Adv. Quantum Chem.* **21** 255
[3] Becke A D 1988 *Phys. Rev.* A **38** 3098
[4] Perdew J P 1986 *Phys. Rev.* B **33** 8822
[5] Becke A D 1993 *J. Chem. Phys.* **98** 5648
[6] Stephens P J, Devlin F J, Chabalowski C F and Frisch M J 1994 *J. Phys. Chem.* **98** 11623
[7] Matsuzawa N, Ishitani A, Dixon D A and Uda T 2001 *J. Phys. Chem.* **105** 4953
[8] Appel F, Gross E K U and Burke K 2003 *Phys. Rev. Lett.* **90** 043005
[9] Casida M E, Gutierrez F, Guan J G, Gadea F X, Salahub D and Daudey J P 2000 *J. Chem. Phys.* **113** 7062

[10] Dreuw A and Head-Gordon M 2004 *J. Am. Chem. Soc.* **126** 4007
[11] Dreuw A, Weisman J L and Head-Gordon M 2004 *J. Chem. Phys.* **119** 2943
[12] Savin A 1996 *Recent Developments and Applications of Modern Density Functional Theory* ed J M Seminario (Amsterdam: Elsevier) p 327
[13] Tawada Y, Tsuneda T, Yanagisawa S, Yanai T and Hirao K 2004 *J. Chem. Phys.* **120** 8425
[14] Iikura H, Tsuneda T, Yanai T and Hirao K 2001 *J. Chem. Phys.* **115** 3540
[15] Yanai T, Tew D P and Handy N C 2004 *Chem. Phys. Lett.* **393** 51
[16] Baer R and Neuhauser D 2005 *Phys. Rev. Lett.* **94** 043002
[17] Rudberg E, Salek P, Helgaker T and Agren H 2005 *J. Chem. Phys.* **123** 184108
[18] Jacquemin D, Perpete E A, Scalmani G, Frisch M J, Kobayashi R and Adamo C 2007 *J. Chem. Phys.* **126** 144105
[19] Wong B M and Hsieh T H 2010 *J. Chem. Theory Comput.* **6** 3704
[20] Kamiya M, Sekino H, Tsuneda T and Hirao K 2005 *J. Chem. Phys.* **122** 234111
[21] Sekino H, Maeda Y and Kamiya M 2005 *Mol. Phys.* **103** 2183
[22] Caricato M, Trucks G W, Frisch M J and Wiberg K B 2010 *J. Chem. Theory Comput.* **6** 370
[23] Sato T, Tsuneda T and Hirao K 2005 *J. Chem. Phys.* **123** 104307
[24] Livshits E and Baer R 2007 *Phys. Chem. Chem. Phys.* **9** 2932
[25] Kobayashi R and Amos R D 2006 *Chem. Phys. Lett.* **420** 106
[26] Chiba M, Tsuneda T and Hirao K 2007 *J. Chem. Phys.* **126** 034504
[27] Sini G, Sears J S and Bredas J L 2011 *J. Chem. Theory Comput.* **7** 602
[28] Cai Z L, Crossley M J, Reimers J R, Kobayashi R and Amos R D 2006 *J. Phys. Chem.* B **110** 15624
[29] Vydrov O A and Scuseria G E 2006 *J. Chem. Phys.* **125** 234109
[30] Casida M E 1995 *Recent Advances in Density Functional Methods* ed D P Chong (Singapore: World Scientific) p 155
[31] Bredas J L, Beljonne D, Coropceanu V and Cornil J 2004 *Chem. Rev.* **104** 4971
[32] Cohen A J, Mori-Sanchez P and Yang W 2008 *Science* **321** 792
[33] Zhang X, Li Z and Lu G 2011 *Phys. Rev.* B **84** 235208
[34] Blochl P E 1994 *Phys. Rev.* B **50** 17953
[35] Perdew J P, Burke K and Ernzerhof M 1996 *Phys. Rev. Lett.* **77** 3865
[36] Kresse G and Hafner J 1993 *Phys. Rev.* B **47** 558
[37] Kresse G and Furthmuller J 1996 *Phys. Rev.* B **54** 11169
[38] Refaely-Abramson S, Baer R and Kronik L 2011 *Phys. Rev.* B **84** 075144
[39] Mardalen J, Samuelsen E J, Gautun O R and Carlsen P H 1991 *Solid State Commun.* **77** 337
[40] Grimme S and Parac M 2003 *ChemPhysChem* **3** 292
[41] Jacquemin D, Perpete E A, Scuseria G E, Ciofini I and Adamo C 2008 *J. Chem. Theory Comput.* **4** 123
[42] Blinov L M, Palto S P, Ruani G, Taliani C, Tevosov A A, Yudin S G and Zamboni R 1995 *Chem. Phys. Lett.* **232** 401
[43] Blom P W M, Mihailetchi V D, Koster L J A and Markov D E 2007 *Adv. Mater.* **19** 1551
[44] Brown P J, Thomas D S, Kohler A, Wilson J S, Kim J, Ramsdale C M, Sirringhaus H and Friend R H 2003 *Phys. Rev.* B **67** 064203
[45] Najafov H, Lee B, Zhou Q, Feldman L C and Podzorov V 2010 *Nature Mater.* **9** 938
[46] Liu T and Troisi A 2011 *J. Phys. Chem.* C **115** 2406
[47] Nakatsuka Y, Tsuneda T, Sato T and Hirao K 2011 *J. Chem. Theory Comput.* **7** 2233